Anomalous growth and properties of $SrTiO_3$-$NaNbO_3$ superlattices

J. Narkilahti, M. Plekh, J. Levoska, and M. Tyunina*
Microelectronics and Materials Physics Laboratories, University of Oulu, PL 4500, FI-90014 Oulun yliopisto, Finland
(Received 22 October 2008; revised manuscript received 10 December 2008; published 12 January 2009)

Epitaxial multilayers and superlattices of quantum paraelectric perovskite $SrTiO_3$ and $NaNbO_3$ constituents with excellent lattice match are grown by pulsed laser deposition on MgO and $LaAlO_3$ substrates using an $La_{0.5}Sr_{0.5}CoO_3$ bottom electrode. Pseudomorphic growth of superlattices is demonstrated for the period as large as 40 nm. With decreasing period below ~20 nm, increase in unit-cell volume exceeding those of bulk constituents and their solid solutions is found. Superlattices exhibit both out-of-plane (normal to substrate surface) and in-plane (parallel to substrate surface) insulating behavior, and decrease in the out-of-plane dielectric permittivity with decreasing period. The results are discussed in terms of possible lattice distortion at the $SrTiO_3$:$NaNbO_3$ interface due to ionic charge mismatch between constituents. Presence of high-permittivity interfacial layers is suggested to be responsible for the evolution of permittivity with decreasing superlattice period.

DOI: 10.1103/PhysRevB.79.014106 PACS number(s): 68.65.Cd, 77.80.−e, 77.90.+k

I. INTRODUCTION

Studies of ABO_3-type perovskite ferroelectric (FE) thin films, performed worldwide since 1960's and greatly stimulated by realization of FE memory, have led to present remarkable achievements in technology of thin-film FEs and their device applications.[1] In modeling of thin-film FEs, last decade has been strongly influenced by a concept of biaxial in-plane strain s that controls polarization P due to s-P coupling.[2] The misfit strain—temperature, or s-T, phase diagrams of FE films have been predicted to differ from those of bulk FEs.[2,3] Controlling strain allows designing thin-film structures with polarization, dielectric, electromechanical, and other properties not readily obtained in bulk FEs.

In epitaxial films, misfit strain is known to relax with increasing film thickness d above a certain critical thickness d_{crit}.[4] For instance, in perovskite FEs, d_{crit} is about several nanometers for misfit magnitude smaller than 2%.[5] The main mechanism of strain relaxation is through formation of misfit dislocations, although in FE films also other mechanisms are principally possible.[6]

Large unrelaxed strain can be achieved in epitaxial superlattices (SLs) consisting of alternating thin-film layers of two or more constituents with the thickness of each layer smaller than d_{crit}. Such strained FE SLs have been grown since early 1990's.[7] In SL with period Λ smaller than a certain Λ_s, the coherent growth of constituent layers and the considerable increase in polarization[8] or permittivity[9] compared to those in FE films have been demonstrated. In contrast to prediction of strain enhanced permittivity, an increase in permittivity has been observed with decreasing period in SLs with constant strain of constituents.[10] Moreover, such an increase has been detected not only in SLs of FEs, but also in relaxor SLs.[11] It has been suggested that in SL, besides strain, also electrostatic coupling between the layers[12] and a specific form of interface coupling[13] can affect polarization. However, physical phenomena at interfaces between the constituents and their influence on properties of SLs remain experimentally unstudied due to dominant effects of strain in the grown epitaxial SLs.

The present work is aimed at experimental studies of influence of interfaces on properties of FE SLs. To avoid or minimize effects of strain and interfacial coupling of polarization, $SrTiO_3$ (STO) and $NaNbO_3$ (NNO) are chosen as constituent materials for SLs. STO is known to be a quantum paraelectric with lattice parameter of the cubic perovskite cell $a_{STO}=3.905$ Å.High-purity single-crystal NNO has been shown to be a quantum paraelectric too.[14] In thin-film form at zero strain, NNO is expected to adopt a pseudocubic crystal structure[15] with lattice parameter $a_{NNO}\approx 3.908$ Å. Assuming an equal distribution of strain between STO and NNO layers in the stack, a negligibly small in-plane biaxial strain of 0.04% is expected. The excellent match between crystal structure and lattice parameters of STO and NNO layers makes it possible to inspect the role of STO:NNO interfaces separately from that of strain.

It should be mentioned that interfaces between STO and other insulators, such as Mott insulator $LaTiO_3$ and band-insulating $LaAlO_3$, have been found to exhibit unusual properties.[16] Distortions of crystal lattice and reconstruction of electronic structure can be responsible for this.[17,18] The origin of these phenomena has been ascribed to the charge mismatch between A-site (La^{3+} and Sr^{2+}) ions at the interfaces.[17] Also at the STO:NNO interface, an ionic charge mismatch exists.

II. EXPERIMENT

STO and NNO thin films and STO:NNO short-period multilayers were grown on (001) MgO and $LaAlO_3$ (LAO) crystal substrates by *in situ* pulsed laser deposition using a ~100 nm thick $La_{0.5}Sr_{0.5}CoO_3$ (LSCO) bottom electrode. The number N of STO:NNO pairs in the stack was varied from 2 to 128 keeping the total stack thickness constant and equal to ~350 nm. SL period $\Lambda=d_{NNO}+d_{STO}$, with d_{NNO} and d_{STO} being the thickness of NNO and STO layers correspondingly, was varied between 6 and 460 unit cells (u.c.). The ratio between d_{NNO} and d_{STO} was similar in all stacks.

Crystalline phases, orientations, and epitaxial relations of the multilayers were studied by x-ray diffraction (XRD) at

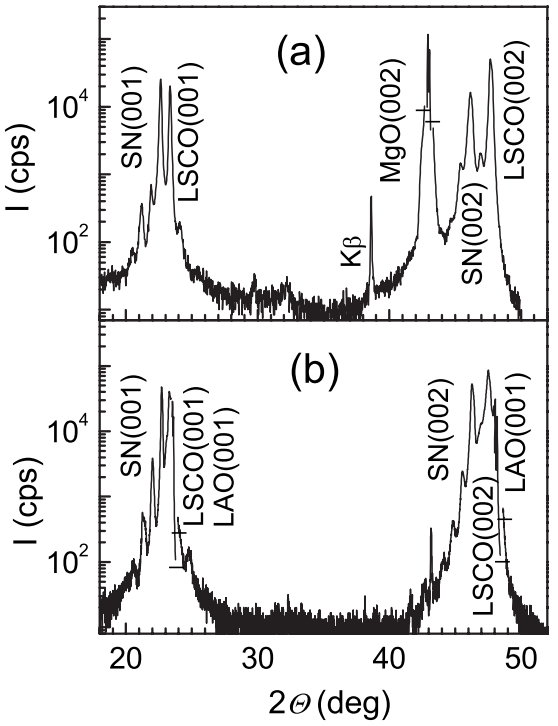

FIG. 1. Θ-2Θ diffraction patterns of STO:NNO superlattices grown on (a) MgO and (b) LSCO substrates.

room temperature. XRD measurements were carried out at Bragg-Brentano type x-ray diffractometer equipped with a postmonochromator and using Cu $K\alpha$ radiation. Θ-2Θ diffraction patterns, ω-2Θ scans and ω-rocking curves were included in XRD study. For reciprocal space mapping, the contribution of $K\alpha_2$ radiation to the total intensity was eliminated by Rachinger correction. The dielectric response of the vertical capacitor structures with Pt top electrodes was measured using an HP4284A LCR meter and Linkam LTSE350 MultiProbe stage. The sheet resistance was tested using four-probe measurements.

III. RESULTS AND DISCUSSION

A. Epitaxial superlattices

The general characteristics of crystal structure and plane orientations are extracted from Θ-2Θ diffraction patterns measured in 2Θ range of 15°–50°. Typical Θ-2Θ XRD patterns of the STO:NNO (SN) multilayers grown on (001) LAO and MgO substrates are shown in Fig. 1. All SN layers are perovskite. The observed (00l)-type reflections of SN layers, LSCO films, and substrates evidence the plane orientation relationship SN(001)‖LSCO(001)‖substrate (001). The maximum volume fraction of (011)-oriented SN material detected in some samples is estimated to be less than 0.5%. Previously, we have made similar observations (011)-oriented material in epitaxial heterostructures of other perovskite films grown on MgO substrates. The performed investigation has revealed that this orientation is formed near the edges of the substrate, where the quality (crystal orientation, smoothness) of substrate surface is distorted. This allows us to treat the major part of the sample surface without considering (011) fraction located at the edges.

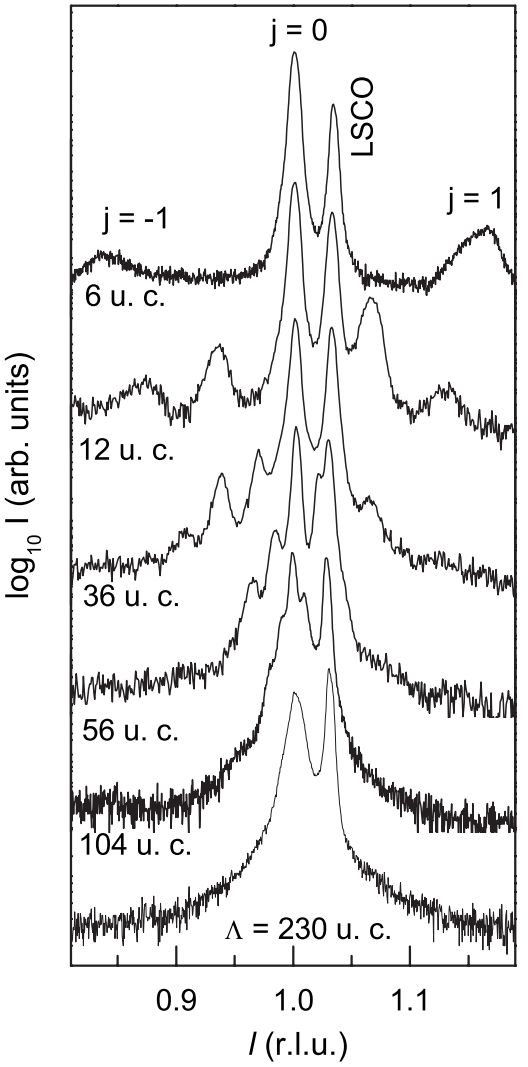

FIG. 2. Evolution of (001) perovskite peak with decreasing period Λ of superlattice from 230 to 6 u.c.

In SLs, periodical arrangement of epitaxial thin layers with different structure factors and/or lattice parameters results in formation of satellite peaks in the vicinity of the main perovskite peak (Θ_0) at the angle interval $\Delta\Theta$ corresponding to the period Λ and order j of the satellite peak. Such peaks indicating formation of SLs are observed for $\Lambda \leq 104$ u.c.. The evolution of Θ-2Θ scans with decreasing period Λ is illustrated for the multilayers grown on LSCO/LAO (Fig. 2). The period Λ is expressed in unit cells with average out-of-plane parameter c. The period is equal to $\Lambda = j/(l_j - l_0)$, where the positions of the satellite and main peaks l_j and l_0 are expressed in relative reciprocal-lattice units (r.l.u.) $2c \sin\theta/\lambda$. Importantly, the superlattice satellite reflections can be clearly seen for Λ as small as 6 u.c., indicating formation of sufficiently abrupt STO:NNO interfaces without noticeable ionic intermixing.

To investigate out-of-plane lattice parameters (normal to the substrate surface) of separate SL constituents, c_{STO} and c_{NNO}, and thicknesses of constituent layers, d_{STO} and d_{NNO},

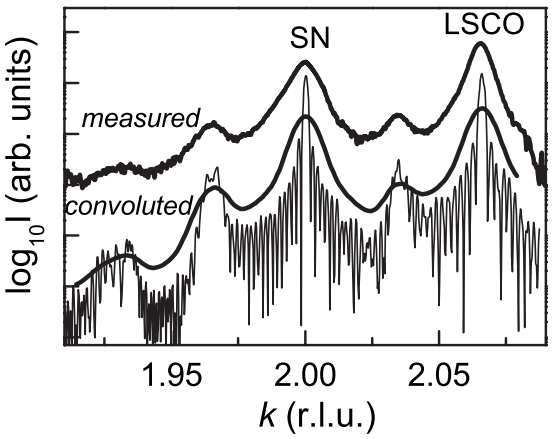

FIG. 3. Simulated (thin line), convoluted, and measured Θ-2Θ diffraction intensity of (002) reflection of superlattice grown on MgO/LSCO.

respectively, the Θ-2Θ XRD patterns of SLs are analyzed using results of numerical simulations. Diffraction intensities along the [00*l*] reciprocal-lattice directions are calculated using the kinematic theory and a set of parameters c_{STO}, c_{NNO}, d_{STO}, and d_{NNO}.[19] The measured and calculated patterns are compared. In Fig. 3, the Θ-2Θ diffraction scan around (002) reflection of SN/LSCO/MgO with $N=32$ is presented together with the results of simulations using $\Lambda=30$ u.c., a 0.8% difference between the lattice parameters $c_{STO}<c_{NNO}$, and asymmetric period $d_{NNO}:d_{STO}=3:1$. The convolution of the calculated intensity assuming a pseudo-Voigt instrumental broadening of 0.055° full width at half maximum (FWHM) is shown too.

Epitaxial quality of multilayers is analyzed using reciprocal space maps derived from ω-2Θ scans in the vicinity of (004) and (024) reflections (Fig. 4). Axes are presented in relative r.l.u., i.e., in reciprocal-lattice indices *k* and *l* for SL average cell. The maxima of LSCO ($l\approx4.09$ in the map) and SL reflections are located in the same (0*kl*) plane confirming the in-plane epitaxial relationship SN[100](001)‖LSCO[100](001). (The epitaxial cube-on-cube growth of LSCO has been previously demonstrated.[19]) The satellite SL peaks are seen both from (004) and (024) reflections. The *k* coordinates of SL (024) maxima are practically the same, indicating similar in-plane lattice parameters (parallel to the substrate surface) of all STO and NNO layers.

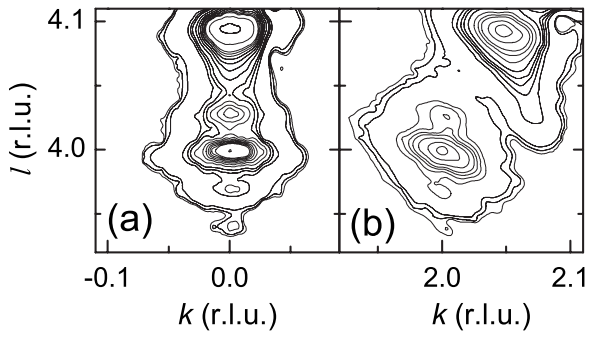

FIG. 4. Reciprocal space maps of the intensity distributions around (a) (004) and (b) (024) reflections on (0*kl*) reciprocal-lattice plane of SN/LSCO/LAO heterostructure with $\Lambda=32$ u.c.

Such a growth with the in-plane lattice parameters being similar in all SL layers of the stack is confirmed by the observed evolution of the (004) reflections in Θ-2Θ scans. The FWHM decreases from about 1° to 0.4°–0.5° with decreasing Λ from 230 to 6 u.c. In SLs, broadening of the XRD peaks due to coexistence of different lattice parameters is absent (or minimum).

The results in Figs. 1–4 evidence epitaxial coherent growth of STO and NNO layers and formation of SLs for $\Lambda\leq104$ u.c.

B. Lattice expansion

In SLs, average out-of-plane lattice parameter *c* is determined using pseudo-Voigt fittings to the main (004) perovskite peak in Θ-2Θ XRD pattern. The in-plane lattice parameters (similar for all layers in SL) are derived from the fittings to (024) reflection using the out-of-plane parameter determined from (004) reflection. In contrast to expectation of strain-free multilayers with $c\approx a\approx3.907$ Å, both the average out-of-plane and the in-plane lattice parameters appeared to be functions of period Λ [Figs. 5(a) and 5(b)].

In the grown heterostructures, the measured in-plane lattice parameter of LSCO layers is about $a_{LSCO}=3.855$ Å. In the stack, the first STO layer grown on the top of LSCO is expected to be compressed in-plane ($a_{LSCO}/a_{STO}-1=3.855/3.905-1=-1.2\%$). For $d_{STO}>d_{crit}$, strain relaxation leads to a_{STO} close to the bulk value. In agreement with this, also in multilayers with $\Lambda>56$ u.c., the in-plane parameter *a* is close to that in bulk STO. With decreasing Λ and correspondingly decreasing d_{STO}, such compressive strain can remain unrelaxed leading to decrease in a_{STO} and, consequently, of common *a* of SL. The observed increase in *a* with decreasing Λ is opposite to this scenario. Assuming that the growth of NNO layers and strong STO:NNO intermixing dominate in increase in *a*, the maximum $a\approx3.91$ Å can be expected.[20,21] The observed $a\approx3.93-3.94$ Å at $\Lambda=6$ u.c. is noticeably larger. Moreover, the increase in *a* is accompanied by a simultaneous increase in the average out-of-plane parameter *c* with the main contribution arising from increase in $c_{NNO}>c_{STO}$ (Fig. 3). It should be noted that the obtained lattice parameters *a* and *c* both exceed those of bulk constituents. Also volume *V* of unit cell of SLs [Fig. 5(c)] exceeds the unit-cell volume of ceramic solid solution 0.75NNO:0.25STO.[21]

In order to eliminate possibility that poor crystal quality has an effect onto observed increase in unit-cell volume, the perfection of crystal plane orientations is characterized using FWHM of ω-rocking curves of (004) and (024) maxima [Fig. 6(a)]. Broader curves obtained on MgO substrates compared to those on LAO substrates are, probably, related to formation of dislocations in LSCO layer. The LSCO:MgO lattice mismatch ($a_{MGO}/a_{LSCO}-1\approx4.21/3.82-1\approx10\%$) is rather large leading to near-substrate formation of misfit dislocations and growth of relaxed LSCO layer. The smaller LSCO:LAO lattice mismatch ($a_{LAO}/a_{LSCO}-1\approx3.79/3.82-1\approx-0.8\%$) results in strain relaxation in LSCO with for-

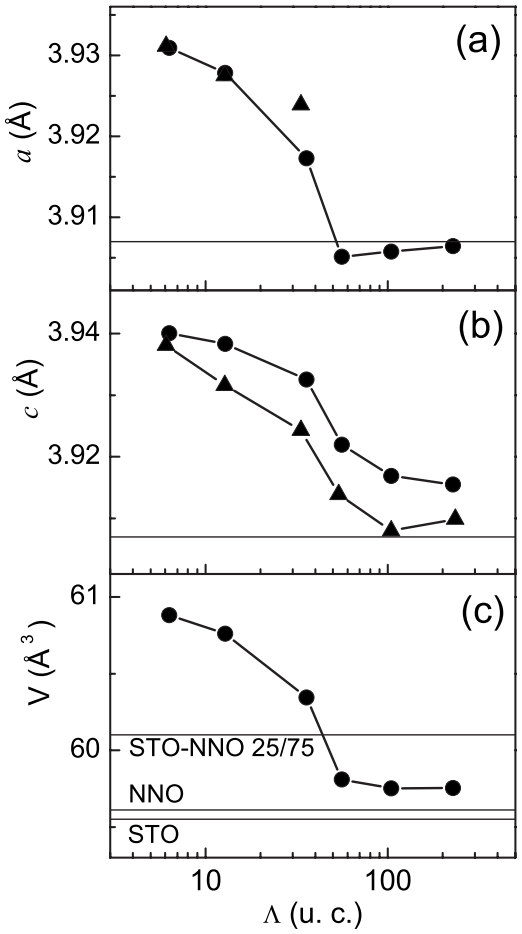

FIG. 5. (a) In-plane lattice parameter a, (b) average out-of-plane lattice parameter c, and (c) unit-cell volume V as a function of period Λ of superlattices grown on MgO (circles) and LAO (triangles) substrates. Expected lattice parameters of superlattice [(a) and (b)] and unit-cell volume determined in films of STO and NNO and in ceramic STO:NNO (c) are also shown.

mation of lower density of dislocations compared to that on MgO. From the net of misfit dislocations, threading dislocations and small-angle grain boundaries can originate, that explains broader ω curves on MgO. However, the FWHM values decrease with decreasing SL period. This tendency is opposite to the increase in unit-cell volume [Fig. 6(b)]. The results in Fig. 6 show absence of correlation between the possible crystal imperfections and the observed lattice expansion.

In perovskite FEs, lattice expansion is principally possible due to presence of oxygen vacancies. It is difficult to directly estimate influence of this factor. Importantly, the lattice expansion has not been found in $(Ba,Sr)TiO_3$ SLs grown using the same process and equipment.[19] Also lattice expansion has not been detected in STO and NNO films, and STO:NNO multilayers with large Λ. This shows that oxygen vacancies can hardly explain the observed increase in V with decreasing Λ.

In SLs, decreasing period Λ with the total thickness of the stack being unchanged means increase in amount of interfaces. The mechanism of lattice expansion is probably related to atomic structure of interfaces.

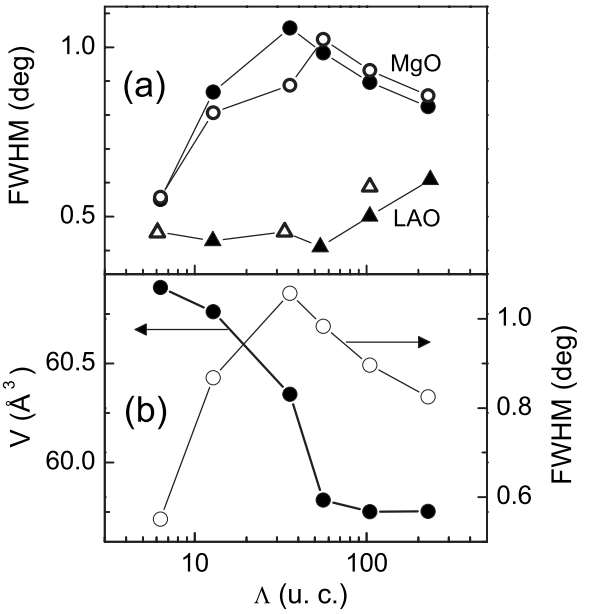

FIG. 6. (a) Full width at half maximum of ω-rocking curves around (004) (solid symbols) and (024) (open symbols) perovskite reflections as a function of period Λ in superlattices grown on MgO (circles) and LAO (triangles) substrates. (b) Unit-cell volume V and FWHM of (004) ω-rocking curve as a function of period Λ in superlattices grown on MgO substrates.

C. $SrTiO_3$:$NaNbO_3$ interface

Considering ABO_3 perovskite structure as a periodic sequence of AO and BO_2 planes, an ideal near-interface region between STO and NNO layers can be presented as a sequence [-NbO_2-NaO-TiO_2-SrO-TiO_2-] and/or [-NbO_2-NaO-NbO_2-SrO-TiO_2-] in the out-of-plane direction of SL. Both the A-site and B-site ions of the constituents have different ionic charges and radii.

Previously, the charge mismatch between A-site La^{3+} and Sr^{2+} ions at the interface between ultrathin $LaTiO_3$ layer and STO substrate has been shown to result in a specific lattice distortion in STO.[17] The largest structural distortions have been revealed in the interface TiO_2 layer. A FE-like relative displacement of the negatively charged O and positively charged Ti ions produces a local ionic dipole moment which screens the Coulomb field created by the substitution of Sr^{2+} by La^{3+} ions. This also leads to an increase in Ti-Ti distance in the out-of-plane direction. Away from the interface, the magnitude of the FE-like distortion decays and the Ti-Ti distance reverts to a constant value close to that in bulk STO.

At the STO:NNO interface, the ionic charge mismatch is more complicated. In Fig. 7, two possible types of near interface region between STO and NNO are shown schematically, with Sr and Na ions at the corners of the cells, and Ti and Nb ions in the centers of the cells. Also oxygen octahedra are shown. Although in perovskite cell the effective charges of ions[22] differ from those tabulated in Ref. 23, the ratio between them can be qualitatively understood using the nominal valences. As shown in Fig. 7, besides ionic mismatch at A site (Na^{+1} and Sr^{+2}), also mismatch at B site exists (Ti^{4+} and Nb^{5+}).

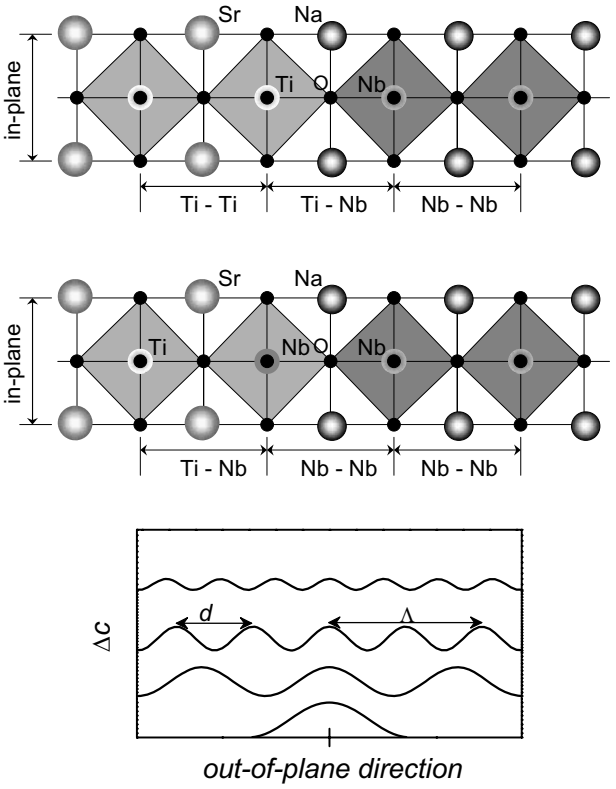

FIG. 7. Schematics of [(a) and (b)] crystal structure at STO:NNO interfaces and (c) evolution of out-of-plane lattice elongation with decreasing period of hypothetical symmetric superlattice (equal thicknesses d of component layers: $\Lambda=2d$). In (c), position of inspected interface is marked on x axis.

The lattice distortions at STO:NNO interfaces [Figs. 7(a) and 7(b)] require first-principles analyses. However qualitatively, it is clear that the Coulomb field can be created by the substitution of Na^{+1} by Sr^{2+} and of Ti^{4+} by Nb^{5+}. To screen this field, possibly either B-site or A-site ions, or both types of ions should be displaced. Similarly to the increase in Ti-Ti distance in the out-of-plane direction at $LaTiO_3$:STO interface, also an increase in interionic distances in the out-of-plane direction at STO:NNO interface can be expected. In the studied STO:NNO SLs, the out-of-plane lattice elongation is found mainly in NNO layers as follows from the comparison to simulations. This indicates possibly stronger effect of Na:Sr substitution on the NNO side compared to that of Ti:Nb substitution on the STO side.

Moving away from the interface, the magnitude of the lattice elongation has been shown to decay,[17] with the thickness of the distorted layer being about 4 u.c. on one side of interface. In SLs in contrast to the single interface considered in Ref. 17, an additional influence of the neighboring interfaces should be taken into account. It is possible to expect that with decreasing SL period Λ and out-of-plane spacing d between interfaces [equal to thickness(es) of constituent layers], each of interfaces will experience stronger influence of the nearest-neighboring interfaces and also of increasing amount of interfaces. Both the magnitude of lattice elongation Δc and thickness of distorted regions can increase with decreasing period. In Fig. 7(c), an evolution of the out-of-plane elongation with decreasing Λ is illustrated for a symmetric SL. For large Λ, the distortion is located near the interface (the lowest curve). With decreasing Λ, the magnitude and spread of this distortion increase, resulting in overall increase in Δc. In STO:NNO SLs, the observed increase in the average out-of-plane lattice parameter c with decreasing Λ [Fig. 5(b)] is in agreement with this scenario.

In the calculations,[17] only the out-of-plane lattice distortions are allowed, with the in-plane lattice parameters of constituents fixed (equal to those of bulk STO). Such an assumption is justified for ultrathin epitaxial layers. It is also valid for SLs built of constituents with noticeable lattice mismatch and minor effect of ionic charge mismatch. In contrast, the growth of the studied STO:NNO SLs can be strongly influenced by ionic charge mismatch. Also assuming not only "face-to-face" interaction of ions, but also their "chessboard-type" interactions, one might expect an appearance of in-plane component of lattice distortion in STO:NNO SLs. The in-plane lattice distortion is found to be noticeable in SLs with $\Lambda \leq 32$ u.c. [Fig. 5(a)]. An additional contribution to the in-plane distortion can be connected with interfacial ionic intermixing and corresponding presence, for instance, of both Sr and Na ions in AO planes. The effect, however, seems to be weak since clear SL satellite peaks are detected for SLs with Λ as small as 6 u.c. (Fig. 2).

In STO:NNO SLs, the observed increase in the average unit-cell volume with decreasing period Λ can be explained by distortion of the perovskite structure caused by ionic charge mismatch at the STO:NNO interface.

The specific arrangement of atomic planes at the interfaces [Fig. 7] can be compared with ionic ordering in bulk perovskites, such as for example Sc:Nb ordering in $PbSc_{0.5}Nb_{0.5}O_3$. Also in ceramic NNO:STO solid solutions, possibility for some degree of Na:Sr and/or Nb:Ti short-range order, which can affect the volume, has been considered.[21] However, the corresponding volume variations have not been detected.

D. Dielectric properties

At the STO:$LaTiO_3$ interface, the ionic charge mismatch has been suggested to result in onset of metallic behavior in the near-interface region with thickness of 2–4 u.c.[16–18] Assuming similar possibility at the STO:NNO interface, the STO:NNO multilayers and SLs can be presented as vertical stacks of STO and NNO layers separated by interfacial in-plane conducting sheets. The interfacial in-plane resistance can differ from the out-of-plane resistance of the stack.

In STO:NNO SLs, the dc resistance measured using neighboring capacitors (connected by the common bottom LSCO electrode and supposedly conducting interfaces) is several tens of MΩ. The resistance remains large under applied electric field, with the breakdown field >30 MV/m in SLs with $\Lambda \geq 32$ u.c. The four-probe measurements do not reveal any noticeable in-plane conductance. The results indicate that in STO:NNO SLs, the interfaces between constituent layers are not conducting. The resistivity ρ of SLs found from the out-of-plane dc resistance is about $\rho \sim (3-9) \times 10^7$ Ω m.

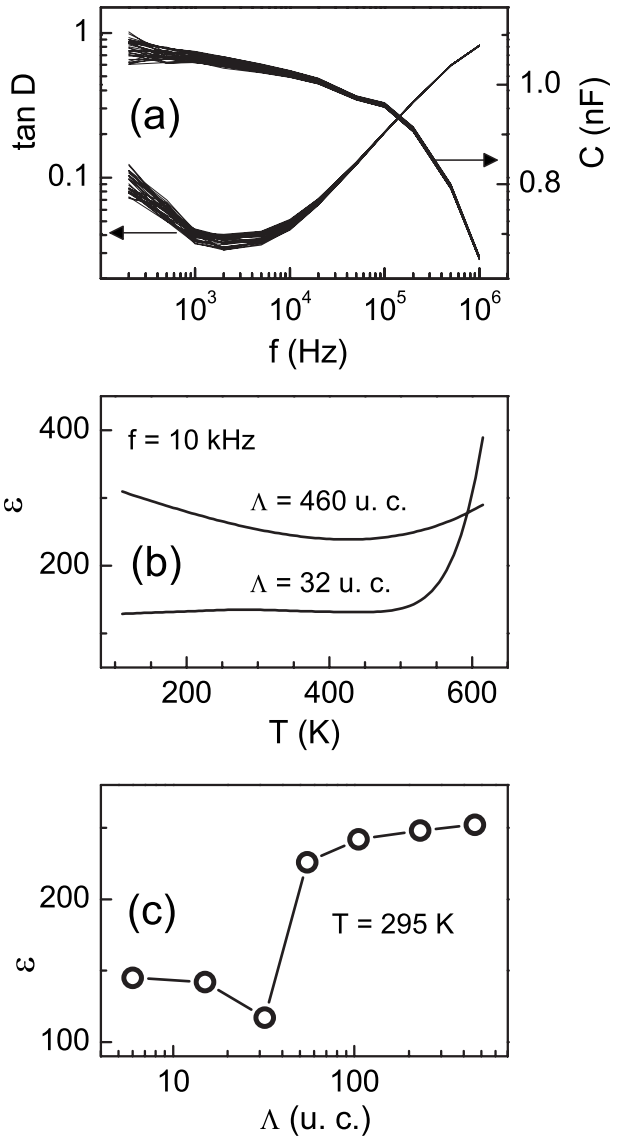

FIG. 8. The out-of-plane ac response of STO:NNO heterostructures. (a) The room-temperature capacitance C and loss tan D as a function of frequency f measured in SL with $\Lambda=12$ u.c. at the amplitude of ac field $10^3-8\times10^6$ V/m. [(b) and (c)] The permittivity ε as a function of (b) temperature and (c) period Λ determined at frequency 10 kHz.

In the out-of-plane impedance measurements[24] using ac electric field, the low-frequency loss factor tan D is determined mainly by the out-of-plane resistance of SL. By comparing the measured impedance with the results of simulations,[24] the capacitance and resistance of the STO:NNO stack can be estimated. In all STO:NNO heterostructures, the frequency-dependent ac response [Fig. 8(a)] resembles that of various previously studied FE thin-film capacitors with LSCO and Pt electrodes.[24] The resistivity estimated from the low-frequency behavior of tan D is about $\rho \sim 10^7$ Ω m, and it remains unchanged with increasing amplitude of ac field to ~8 MV/m. The good agreement between the dc and ac resistivity of SLs confirms the absence of interfacial conductance.

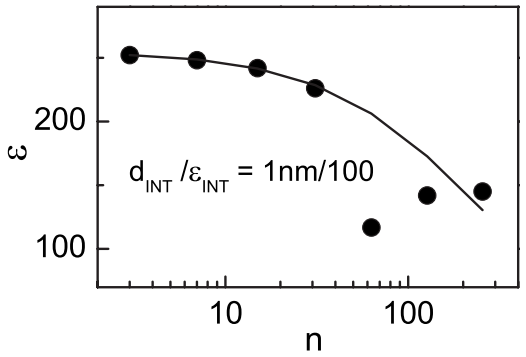

FIG. 9. The room-temperature dielectric permittivity ε measured in STO:NNO SLs as a function of number n of STO:NNO interfaces. Solid line shows fit to expression (1).

From the measured capacitance, the real part ε of the average out-of-plane dielectric permittivity is extracted. In the grown SNO:NNO SL heterostructures, the measured ε is practically temperature independent below 450 K [Fig. 8(b)].[25] The room-temperature permittivity tends to decrease with decreasing Λ [Fig. 8(c)]. This is in contrast to the relative increase in ε in bulk NNO:STO solid solutions with increasing STO content.[26,27] Also this is in contrast to the enhanced ε usually observed in SLs.

In the STO:NNO SLs, due to the lattice expansion, the permittivity of each of the constituents can differ from that of their prototypes, and it is not known. The out-of-plane dielectric and possible FE (Ref. 17) properties of the near-interface layers are not known either. This makes it difficult to analyze the response of SLs. To qualitatively estimate possible influence of interface layers on the dielectric response, the vertical SL capacitor heterostructure is presented as a series connection of NNO, STO, and interface capacitors. The permittivity of SL with interfaces, ε_{SL+INT}, can be described by

$$\frac{1}{\varepsilon_{SL+INT}} \approx \frac{1}{\varepsilon_{SL}} + n\frac{d_{INT}}{d}\left(\frac{1}{\varepsilon_{INT}} - \frac{1}{\varepsilon_{SL}}\right), \qquad (1)$$

where n is the number of similar interface layers of thickness d_{INT} and permittivity ε_{INT}, and d is the total thickness of the stack. The permittivity ε_{SL} would be measured in the stack without interfacial layers. As seen from Eq. (1), the drop of ε_{SL+INT} with decreasing Λ (increasing n) is possible for $\varepsilon_{INT}<\varepsilon_{SL}$. Indeed, a satisfactory fit of ε measured in the grown stacks to expression (1) is obtained for $\varepsilon_{INT}=100$ and $\varepsilon_{SL}=250$ [Fig. 9].

Although the permittivity of constituents and interfaces might vary with n, the approximation (1) can qualitatively explain the change in permittivity as a function of SL period. It should be noted that in SLs with the relatively small difference between ε_{INT} and ε_{SL}, a noticeable change of ε_{SL+INT} can be obtained due to large number of interfaces. The permittivity of such interfaces can be high, in contrast to the low permittivity of the film-electrode interface, commonly considered in FE thin-film heterostructures.[28,29] Remarkably, assuming a large ε_{INT} exceeding that of the constituents, ε_{INT}

$>\varepsilon_{SL}$, the expression (1) could also explain often observed tendency of ε_{SL+INT} to increase with decreasing Λ.

In STO:NNO SLs, interfaces with large ε_{INT}, which slightly differs from that of constituents, can exist due to the near-interface structural distortions caused by the discussed ionic charge mismatch. Since the corresponding interfacial phase can possess FE-like out-of-plane polarization, the permittivity of such interface layer can be smaller than that of the paraelectric constituents: $\varepsilon_{INT}<\varepsilon_{SL}$, leading to the observed evolution of ε [Fig. 9].

E. Superlattices and ultrathin films

The present study reveals the influence of ionic charge mismatch on growth and properties of perovskite FE SLs. In previous studies of epitaxial FE thin films and SLs, the effect of charge mismatch has remained practically unnoticed due to usually dominating influence of the lattice mismatch and associated in-plane misfit strain. Indeed, the out-of-plane lattice expansion induced by charge mismatch is difficult either to detect at presence of an in-plane tensile strain or to separate from the strain induced lattice elongation at the presence of an in-plane compressive strain. It should be mentioned, however, that an additional out-of-plane elongation found in compressively strained epitaxial STO films grown on $NdGaO_3$ substrates[30] might be related to ionic Sr^{2+}:Nd^{3+} mismatch.

In perovskite FEs, same ions or ions with similar nominal valences possess different effective charges.[22] (For instance, effective charges of Ba in $BaTiO_3$ and of Sr in SrTiOr are not equal to +2 and differ from each other.) In perovskite FE SLs with atomically abrupt interfaces between constituent layers, ionic charge mismatch can exist. Correspondingly, the near-interface regions of several unit cells in thickness can possess specific atomic displacements and electrical properties, different from those inside constituents. The presence of an interfacial dielectric layer with $\varepsilon_{INT}\neq\varepsilon_{SL}$ can contribute to the change of SL permittivity with decreasing Λ [Eq. (1)].

Additionally, in epitaxially strained perovskite FE SLs, adjacent constituent layers can possess different signs of biaxial in-plane strain and different magnitudes and directions of polarization. At the interface between such layers, a gradual change in polarization can lead to the formation of ultrathin near-interface layer with permittivity different from that of either of the constituents. Also such layers can influence the evolution of SL permittivity with decreasing Λ [Eq. (1)].

The properties of FE SLs can be simultaneously affected by lattice mismatch, polarization couplings, and ionic charge mismatch. With decreasing SL period, changes in dielectric behavior seem to be associated mainly with interfacial phenomena.

The discussed possible formation of specific near-interface layers suggests that for an ultrathin perovskite layer, with thickness of several unit cells and sandwiched between other perovskite layers, the crystal and electronic structures are inhomogeneous. Currently, neither phenomenological nor first-principles analyses of ultrathin films[31] take this into account.

IV. CONCLUSIONS

The growth of epitaxial SL heterostructures of alternating $SrTiO_3$ and $NaNbO_3$ layers on $La_{0.5}Sr_{0.5}CoO_3$ bottom electrode layer and MgO or $LaAlO_3$ substrates is experimentally demonstrated for the period as large as 40 nm. With decreasing period below ~20 nm, increase in unit-cell volume exceeding those of bulk $SrTiO_3$, $NaNbO_3$, and $SrTiO_3$-$NaNbO_3$ solid solution is observed. In the heterostructures, insulating behavior is detected both in out-of-plane and in-plane directions. The out-of-plane dielectric permittivity is found to decrease with decreasing period.

The observed lattice expansion and dielectric properties are explained by possible lattice relaxation at the STO:NNO interface resulting from Sr:Na and/or Ti:Nb ionic charge mismatch. Presence of high-permittivity interfacial layers is suggested to be responsible for the evolution of SL permittivity with decreasing period.

ACKNOWLEDGMENTS

The authors acknowledge Academy of Finland (J.N., Project No. 118250), Infotech Oulu Graduate School (M.P.), EU FP6 (Project No. 027468), COST 539 ELENA, and EMPART Group of Infotech Oulu for support.

*Corresponding author; marinat@ee.oulu.fi

[1] M. Dawber, K. M. Rabe, and J. F. Scott, Rev. Mod. Phys. **77**, 1083 (2005) and references therein; N. Setter, D. Damjanovic, L. Eng, G. Fox, J. Appl. Phys. **100**, 051606 (2006).

[2] N. A. Pertsev, A. G. Zembilgotov, and A. K. Tagantsev, Phys. Rev. Lett. **80**, 1988 (1998).

[3] O. Dieguez, S. Tinte, A. Antons, C. Bungaro, J. B. Neaton, K. M. Rabe, and D. Vanderbilt, Phys. Rev. B **69**, 212101 (2004); I. Kornev, H. Fu, and L. Bellaiche, Phys. Rev. Lett. **93**, 196104 (2004).

[4] See, e.g., M. Ohring, *The Materials Science of Thin Films* (Academic, New York, 2002).

[5] F. He, B. O. Wells, and S. M. Shapiro, Phys. Rev. Lett. **94**, 176101 (2005).

[6] J. S. Speck and W. Pompe, J. Appl. Phys. **76**, 466 (1994).

[7] K. Iijima, T. Terashima, Y. Bando, K. Kamigaki, and I. Terauchi, J. Appl. Phys. **72**, 2840 (1992).

[8] H. N. Lee, H. M. Christen, M. F. Chisholm, C. M. Rouleau, and D. H. Lowndes, Nature (London) **433**, 395 (2005).

[9] H. Tabata, H. Tanaka, and T. Kawai, Appl. Phys. Lett. **65**, 1970 (1994).

[10] M. Tyunina, I. Jaakola, J. Levoska, and M. Plekh, Phys. Rev. B **76**, 134107 (2007).

[11] M. H. Corbett, R. M. Bowman, J. M. Gregg, and D. T. Foord, Appl. Phys. Lett. **79**, 815 (2001).

[12] A. L. Roytburd, S. Zhong, and S. P. Alpay, Appl. Phys. Lett. **87**,

092902 (2005); V. A. Stephanovich, I. A. Luk'yanchuk, and M. G. Karkut, Phys. Rev. Lett. **94**, 047601 (2005); K. Johnston, X. Huang, J. B. Neaton, and K. M. Rabe, Phys. Rev. B **71**, 100103(R) (2005).

[13] E. Bousquet, M. Dawber, N. Stucki, C. Lichtensteiger, P. Hermet, S. Gariglio, J.-M. Triscone, and P. Ghosez, Nature (London) **452**, 732 (2008).

[14] S. I. Raevskaya, I. P. Raevski, S. P. Kubrin, M. S. Panchelyuga, V. G. Smotrakov, V. V. Eremkin, and S. A. Prosandeev, J. Phys.: Condens. Matter **20**, 232202 (2008).

[15] O. Dieguez, K. M. Rabe, and D. Vanderbilt, Phys. Rev. B **72**, 144101 (2005).

[16] See, e.g., S. A. Pauli and P. R. Willmott, J. Phys.: Condens. Matter **20**, 264012 (2008) and references therein.

[17] S. Okamoto, A. J. Millis, and N. A. Spaldin, Phys. Rev. Lett. **97**, 056802 (2006).

[18] D. R. Hamann, D. A. Muller, and H. Y. Hwang, Phys. Rev. B **73**, 195403 (2006).

[19] I. Jaakola, J. Levoska, and M. Tyunina, J. Appl. Phys. **102**, 014108 (2007).

[20] Y. I. Yuzyuk *et al.*, J. Phys.: Condens. Matter **17**, 4977 (2005).

[21] H. Xu, A. Navrotsky, Y. Su, and M. L. Balmer, Chem. Mater. **17**, 1880 (2005).

[22] W. Zhong, R. D. King-Smith, and D. Vanderbilt, Phys. Rev. Lett. **72**, 3618 (1994).

[23] *CRC Handbook of Chemistry and Physics*, 79th ed., edited by D. R. Lide (CRC Press, Boca Raton, Florida, 1998).

[24] M. Tyunina, J. Phys.: Condens. Matter **18**, 5725 (2006).

[25] The detailed study of the electrical properties will be published elsewhere.

[26] N. N. Krainik, Izv. Akad. Nauk SSSR, Ser. Fiz. **22**, 1492 (1958).

[27] T. Hungria, M. Alguero, and A. Castro, Chem. Mater. **18**, 5370 (2006).

[28] N. A. Pertsev, R. Dittmann, R. Plonka, and R. Waser, J. Appl. Phys. **101**, 074102 (2007) and references therein.

[29] L. J. Sinnamon, R. M. Bowman, and J. M. Gregg, Appl. Phys. Lett. **78**, 1724 (2001).

[30] T. Yamada, J. Petzelt, A. K. Tagantsev, S. Denisov, D. Noujni, P. K. Petrov, A. Mackova, K. Fujito, T. Kiguchi, K. Shinozaki, N. Mizutani, V. O. Sherman, P. Muralt, and N. Setter, Phys. Rev. Lett. **96**, 157602 (2006).

[31] See, e.g., I. Ponomareva, L. Bellaiche, and R. Resta, Phys. Rev. Lett. **99**, 227601 (2007).